Exploring the role of NAD+ metabolism in response to mitochondrial respiratory chain inhibition

Synopsis of PhD research work

Ankita Sarkar

Enrolment No. – PU/PHD/DLS/2018/011

Registration No.- R-18RS18220146

Supervisor: Dr. Piyali Mukherjee

Laboratory of Molecular Neurodegeneration & Aging Research

Institute of Health Sciences

(Erstwhile School of Biotechnology)

Presidency University

Kolkata

Name: Ankita Sarkar

Supervisor: Dr. Piyali Mukherjee

Current Designation: Assistant Professor & Coordinator, Institute of Health Sciences
Presidency University, Kolkata

Title of the Thesis: Exploring the role of NAD+ metabolism in response to mitochondrial respiratory chain inhibition

PhD Registration No.: R-18RS18220146

Enrolment No.: PU/PHD/DLS/2018/011

Place of work: Institute of Health Sciences (erstwhile School of Biotechnology), Presidency University (2nd Campus), Plot No. DG/02/02, Action Area-ID New Town (Near Biswa Bangla Convention Centre) Kolkata-700156, West Bengal, India.

Residential Address: 98/2, Tripura Roy Lane, Salkia, Howrah-711106.

Mailing Address: 98/2, Tripura Roy Lane, Salkia, Howrah-711106.

Email: ankitasarkar2702@gmail.com

Research Scholar

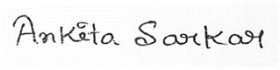

(Full Signature)

Forwarded

Supervisor:

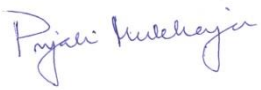

(Full Signature)

Date:

Exploring the role of NAD+ metabolism in response to mitochondrial respiratory chain inhibition

Introduction:

Nicotinamide adenine dinucleotide (NAD^+) is an essential metabolite that acts as a redox co-factor, a transcriptional regulator and a key determinant of energy status under different physiological condition[1 2 3]. Deregulation of NAD^+ homeostasis has been observed in several pathological conditions such as cancer, neurodegeneration and diabetes[4 5 6]. The NAD^+-consuming enzymes like PARPs, Sirtuins, CD38 and Sarm1[7 8 9] has been shown to play an important role in the regulation of NAD^+ homeostasis and regulate different cellular functions that includes DNA damage repair, transcriptional regulation, neurodegeneration, autophagy and apoptosis[10 11 12 13]. Compartmentalization of NAD^+ is of key interest as NAD^+ levels within the various cellular organelles is intricately associated with the regulation of cell death and survival[14 15]. Mitochondria harbours the largest NAD^+ pool as NAD^+ can be regenerated within these organelle via the electron transport chain (ETC) [16 17] and dysregulation of mitochondrial activity by respiratory complex chain inhibition is the hallmark of several life-threatening conditions[18]. Mitochondrial complex I is the first point of entry of electrons resulting in the oxidation of NADH to NAD^+ [19]. Inhibition of mitochondrial complex I activity has been shown to be linked with increase in reactive oxygen species (ROS) accumulation and mitochondrial dysfunction. However, how these phenomena are linked to energy deficits within the cells via NAD^+ regulation is not clearly understood.

PARP1, a member of the PARP family of proteins, is one of the well-studied NAD^+ consuming enzymes. While the short-term activation of PARP1 triggers a DNA damage response that is considered to be crucial for maintaining cellular homeostasis, prolonged activation of PARP1 may cause rapid degradation of NAD^+ and eventual cell death[20 21 22 23]. Inhibition of PARP1 by its potent inhibitors like PJ34 or Olaparib plays a crucial role in preventing disease progression and is currently a major strategy for anti-cancer therapeutics[24 25]. PARP1 has been shown to limit the level of NAD^+ that may affect the activity of two other NAD^+ dependent enzymes Sarm1 and Sirtuins[26 27]. Interestingly, the newly discovered NADase, Sarm1 known for its pro-neurodegenerative roles, is also allosterically regulated by NAD^+ levels within the cells [28 29]. The study provides an important understanding of temporal regulation of key cellular processes by fluctuating NAD^+ levels following mitochondrial complex I inhibition by rotenone and the importance of PARP inhibitors in this process.

Objectives of the study:

- **To investigate the role of NAD^+ metabolism and the effect of PARP inhibition in response to mitochondrial respiratory complex-I inhibition**
- **Repurposing PARP1 inhibitors as therapeutic strategy in the context of neurodegenerative diseases**

Hypothesis:

Hyperactivation of PARP1 in response to mitochondrial complex I inhibition is associated with rapid loss of NAD^+ that may lead to Sarm1 activation leading to further NAD^+ loss and ultimately cell death. Inhibition of PARP1 may ameliorate the cell death induced by rotenone by restoring the endogenous NAD^+ levels, and preventing Sarm1 activation.

Materials and methods:

Cell lines-HEK293 and SH-SY5Y cells were obtained from the laboratory of Dr. Abhik Saha (Institute of Health Sciences, Kolkata, India) and Dr. Oishee Chakrabarti (Saha Institute of Nuclear Physics, Kolkata) respectively. The cells were maintained in Gibco's Dulbecco's modified Eagle's medium (DMEM) (11995-065) or low glucose DMEM (11885-084) or phenol red free DMEM (11039-021) from Gibco, supplemented with 10% fetal bovine serum (Invitrogen) and 1% Penicillin-Streptomycin Solution (Sigma).

Antibodies-Antibodies against □-actin (ab8224), p62 (ab56416), total OXPHOS cocktail (ab110411), SIRT1 (ab32441), Cleaved caspase-3 (ab2302), LC3 A/B (ab128025), DNA damage [H2A.X(S139) + cleaved PARP1 + Anti-GAPDH] antibody cocktail (ab131385), anti-Mouse (ab97023) and anti-Rabbit polyclonal secondary antibodies were purchased from Abcam. Antibodies against □-actin (MCA577G), PAR (MCA-1480) were purchased from Bio-Rad. Antibodies against FLAG (MA1-91878), ATP5A1 (15H4C4) and COX IV (PA5-19471) were obtained from Thermo Fisher Scientific. Anti-hGAPDH (DSHB-hGAPDH-2G7), SQSTM/p62 (GTX636328) and Sarm1 (GTX77621) were brought from DSHB and GeneTex respectively. Antibodies against COXIV (11967), Beclin (#3495), PARP1 (#9532), Sarm1 (#13022) were purchased from Cell Signalling Technology Inc.

Chemicals-Mitochondrial complex I inhibitor rotenone (Sigma), pan caspase inhibitor Z-VAD (OMe)-FMK (Abcam), PARP-1 inhibitor PJ-34 hydrochloride (Abcam), SIRT1 inhibitor EX-527 (Abcam), autophagy inhibitor Chloroquine diphosphate salt (Sigma), ROS scavenger N-acetyl cystine (Sigma) were used in this study at the indicated doses. Nicotinamide riboside (NR) was procured from ChromaDex, USA.

Cell viability Assays-Cell viability was measured by MTT and SRB (Sulforhodamine B) assays. Cells were seeded in 24-well (0.4×10^5) and 96-well (0.2×10^5) plates respectively for 24 h and were treated with indicated drugs for indicated time points. Wells in triplicate were incubated with the MTT reagent (Sigma) or SRB reagents by following manufactures' protocol (ab235935). The absorbance was measured at 540 nm and 490 nm respectively in a multiple plate reader (BioTek).

Plasmids and transfections-Cells were seeded at a density of 0.4×10^5 cells/well, 24 h prior to transfection. SH-SY5Y and HEK293 Cells were transfected with pCMV6-Sarm1 with C-terminal Myc-DDK tag (a kind gift from Dr. Karin Peterson, Rocky Mountain Laboratories, NIAID, NIH, USA), GFP-LC3B (a kind gift from Dr. Abhik Saha, Institute of Health Sciences, Kolkata, India), construct Mito-mRFP-EGFP (a kind gift from Dr. Benu Brata Das, IACS, Kolkata, India), siPARP1 (100 nM, #6304, Cell Signalling Technology lnc.), siSARM1 (25 nM, s23032, Ambion, life technologies), and siSIRT (50 nM, #s223591, Thermo Fisher Scientific) with Lipofectamine 2000 (Invitrogen) for 48 h by using the manufacturer's protocol.

Immunoblot Analysis-were cultured in 6-well plates at a density of 0.3×10^6 per well 24 h prior to treatment as indicated. Following treatment, whole cell lysate was prepared in lysis buffer (150 mM NaCl, 1% NP-40, 50mM Tris pH 8.0 plus protease inhibitors). Protein concentration was estimated using the Bradford assay kit (Bio-Rad) and 15 □g of protein/well were resolved on 12% SDS-PAGE and subsequently analysed by immunoblot analysis. Bands were detected by a chemiluminescent ECL system (Bio-Rad) and quantified by Image J software.

Immunofluorescence assay–Cells were seeded at a density of 3×10^4 cells/well 24 h prior to the treatment. Cells were fixed (4% p-formaldehyde), permeabilised and blocked for 30 mins followed by incubation with primary antibody at 4°C overnight. Then probed with secondary antibody (Alexa flour 488/594) along with DAPI (Bio-Rad) for 1 h at room temperature and mounted with Fluoroshield (Abcam) and sealed for analysis. In case of live staining the cells were seeded in grooved 35 mm plates at a density of 0.02×10^6. Next, cells were incubated with Lysotracker red DND9, Mitotracker green FM, TMRM (Sigma), Mitosox and Hoechst 33342 (Sigma) at 37°C for 20 min and analysed by confocal microscope. In case of Phalloidin (Invitrogen A22283) staining the fixed cells were incubated with anti-F-actin conjugated to Phalloidin

(1:200) and DAPI for 1 h. All images were acquired by DMi8 confocal laser scanning microscope (Leica-microsystems) and images were analysed using image J software.

NAD^+/NADH Assay-Total NAD concentration, NAD^+/NADH ratio and the concentration of total NAD^+ and NADH was determined by NAD/NADH fluorometric and colorimetric assay kit from Abcam (ab176723, fluorometric assay), (ab65348, colorimetric assay) by following manufacture's protocol. Respective concentrations were calculated by the equation Total (NAD/NADH) = (B/V) x D where B = total NAD/NADH amount in the sample well (pmol), V=sample volume added in the sample wells (µl), D= sample dilution factor. The NAD^+/NADH ratio is calculated as: ratio= (NAD_{TOTAL}-NADH)/NADH.

ATP ASSAY-The cellular ATP level was determined by ATP determination kit from Molecular Probes (A22066). The ATP levels were expressed as nmoles of ATP /µg of protein.

cADPR Assay- The concentration of cADPR was measured by Amplite Fluorometric cADPR-Ribose Assay Kit (20305) from AAT Bioquest. The fluorescence intensity was monitored at an Ex/Em=420/480 nm. cADPR concentration for the test samples was expressed as µg of cADPR/mg of protein.

Mitochondrial fractionation- Mitochondrial fractions for both the cell lines were collected by using Mitochondrial Isolation Kit for Cultured Cells from Abcam (ab110170). Briefly, $2.2x10^6$ cells were seeded in a 100 mm plate 24 h prior to treatment. Cells were treated at a confluency of 70% and kept for 24 h. Cells were resuspended in solution A and B respectively then homogenized and centrifuged. Intact mitochondrial pellets and supernatants (cytosol) were collected for each sample and stored at -80° C for future purpose. Mitochondrial protein content was estimated by DC protein assay kit.

Complex I activity assay- Mitochondrial complex I activity was determined by Mitochondrial complex I activity colorimetric assay kit (ab287847) from Abcam. 5 µg of mitochondrial protein was used from every sample to perform the assay. The absorbance at 600 nm were measured in kinetic mode at an interval of 1 min by BIOTEK Synergy H1 plate reader at room temperature for up to five minutes.

Measurement of total cellular ROS – Intracellular ROS was measured by H2DCF-DA (Sigma, D6883). After treatment, cell lysate was prepared lysis buffer and 50 µM H2DCFDA was added and incubated for 1 h and fluorescence intensities were measured at Ex/Em: 492/527 nm by plate reader.

qReal-Time PCR – RNA samples were collected by standard PureZol RNA isolation solution (Biorad) and cDNA was prepared by Bio-Rad's iScript cDNA synthesis kit. To analyse dSarm expression, fly heads were collected from young flies at day 5 of rotenone treatment in the presence or absence of Olaparib and crushed in a mortar-pestle with TRIZOL. The real-time data was analysed and quantified by CFX manager software (Bio-Rad). All the results were obtained from at least three independent experiments.

Fly survival and negative geotaxis assay-W^{1118} flies were a generous gift from Dr. Rupak Dutta, IISER, Kolkata. Both male and female flies were grown at 22° C and 12-h light/dark cycle in incubator in standard corn meal-agar diet. Rotenone and Olaparib was freshly prepared as 100 mM and 10 mM stock solutions in DMSO. Flies were transferred to rotenone or Olaparib containing medium every 2-3 days to monitor survival and locomotor deficit. The total number of flies along with the dead and viable ones were counted at 3-day interval and the percentage of survival was calculated up to 20 days for each set. The negative geotaxis assay was performed in a similar manner to that published by Gargano *et al* (Gargano et al., 2005) with minor modifications.

Fly brain staining- The adult fly brains were mechanically dissected under stereo zoom microscope (Olympus, Japan). Immediately, the brains were fixed with 4% PFA for 30 minutes followed by an overnight incubation with anti-tyrosine hydroxylase (Merck Millipore) and anti-ELAV in PBT (5% BSA, 0.3% Triton X-100 in PBS) solution. Next, the tissues were incubated with anti-rabbit Alexa 488 and anti-

mouse Alexa 594 secondary antibodies (Sigma) for 3 h and were mounted and sealed. The whole brain images were taken by Leica confocal microscope (DMI8).

Statistical Analysis

All statistical analysis was performed using GraphPad Prism version 7.00 for Windows (GraphPad Software, La Jolla, CA, USA). The results are presented as mean ± SEM (standard error of mean) of at least three independent experiments performed in triplicate. Statistical significance was measured by one-way analysis of variance (ANOVA) with Bonferroni post-test. Asterisks indicate levels of significance (*$p < 0.05$, **$p < 0.01$ and ***$p < 0.001$).

Results and discussion:

Objective I: To investigate the role of NAD^+ metabolism and the effect of PARP inhibition in response to mitochondrial respiratory complex-I inhibition

Mitochondrial complex-I inhibitor rotenone induces cell death in a dose and time dependent manner in both HEK293 and SH-SY5Y cells that is independent of caspase-3 activation

Rotenone is a lipophilic mitochondrial complex I inhibitor that has been associated with sporadic case of Parkinson's disease[30]. Our previous data has revealed that rotenone treatment results in the loss of dopaminergic neurons in *Drosophila melanogaster*. Here, we aimed to gain a comprehensive insight in rotenone mediated cell death in both neuronal SH-SY5Y and non-neuronal cell line HEK293. Our results indicate that rotenone induced ~40% of cell death in HEK293 cells at a dose as low as 500nM (Fig. 1A) but a higher dose (5µM) was required to achieve similar percentage of cell death in SH-SY5Y cells (Fig. 1B). The cell death induced by rotenone was also compared in a sulforhodamine B (SRB) assay that measures

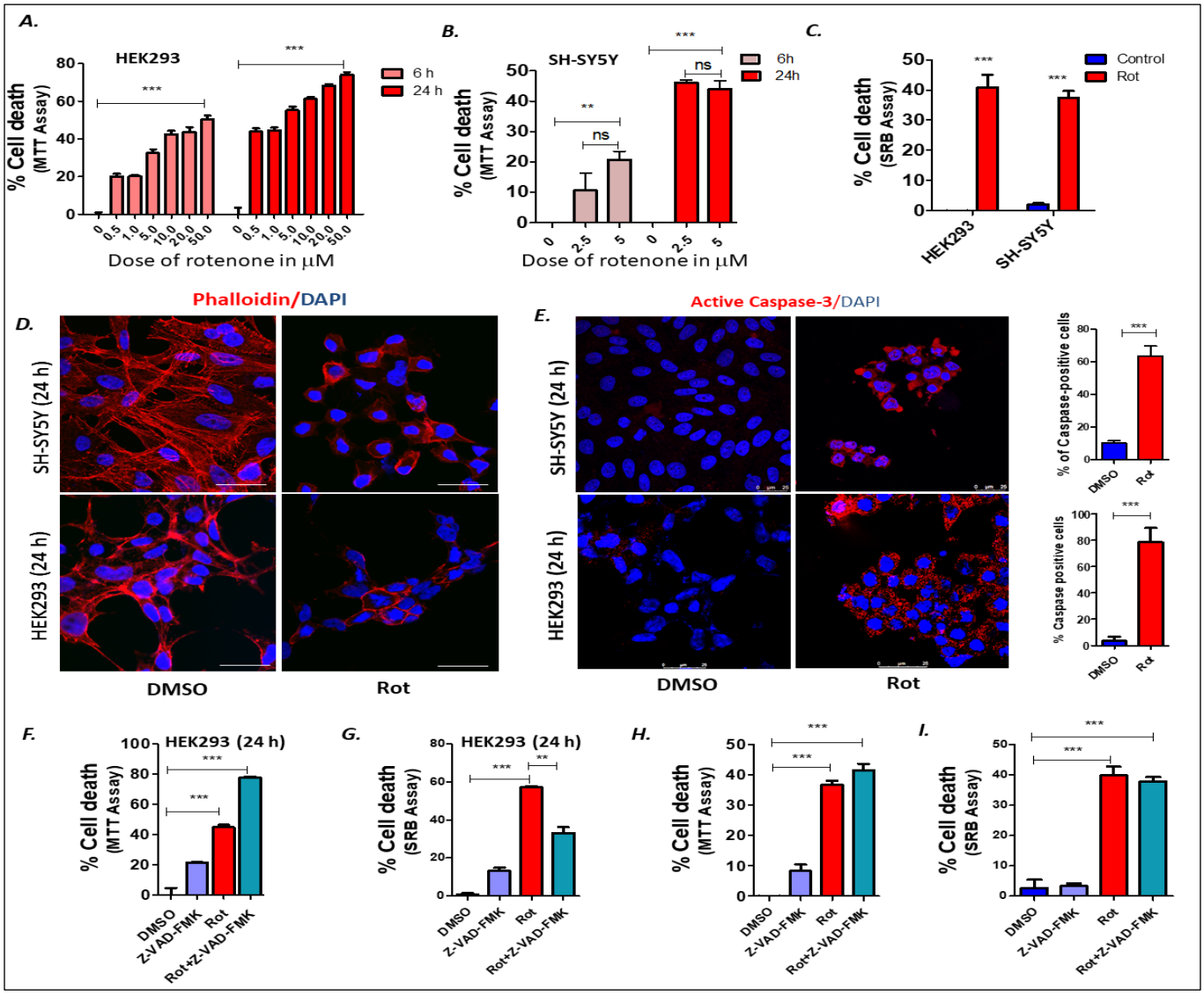

Fig. 1. (A-C) HEK293 and SH-SY5Y cells were treated with rotenone at different doses and cell death was measured by MTT and SRB assays respectively at indicated time points. **(D)** Cells were stained with F-actin conjugated to Phalloidin (red) and DAPI, 24 h post-rotenone treatment. **(E)** Confocal images of SH-SY5Y and HEK293 cells immunostained with active caspase-3 and DAPI, 24 h post-rotenone treatment. Right panel indicates the quantitation of caspase positive cells. **(F-I)** Quantitative analysis of percentage of cell death in HEK293 (F, G) and SH-SY5Y (H, I) cells pre-incubated with pan caspase inhibitor Z-VAD-FMK (20 µM) followed by rotenone treatment.

cellular protein levels (cell mass) as compared to MTT assay that measures the metabolic death rate. The results obtained by SRB assay were comparable with the MTT assay for both HEK293 and SH-SY5Y cells inducing around 40%-50% cell death at the indicated doses (Fig. 1 C). Further, immunofluorescence analysis with F-actin marker conjugated to Phalloidin revealed an overall disruption of the cytoskeletal structure of both the cell lines at 24 h post rotenone treatment (Fig. 1D). To understand the effect of rotenone on cellular morphology in these two cell lines, we stained the cells with F-actin conjugated to Phalloidin and the results indicate an overall disruption of the cytoskeletal structure in both these cell lines following rotenone treatment (Fig. 1 D Upper and Lower Panel). Since rotenone induced ~40% cell death at the indicated doses, we further evaluated the status of apoptosis in both HEK293 and SH-SY5Y cells following rotenone treatment. Rotenone treatment resulted in caspase-3 activation as indicated by increased accumulation of active caspase-3 in the cells treated with 5 μM and 500 nM of rotenone in SH-SY5Y (Fig. 1E Upper Panel) and HEK293 (Fig. 1E Lower Panel) respectively. However, prior incubation with the PAN caspase inhibitor Z-VAD-FMK did not reverse rotenone-induced cell death in these cells in MTT (Fig. 1F and H) assay. However, there was a moderate reversal in cell death in the presence of the caspase inhibitor in HEK293 cells in SRB assay (Fig. 1 G). However, in line with the MTT assay no such reversal could be observed in the SH-SY5Y cells in the SRB assay (Fig. 1I) indicating that caspase activation was perhaps not the sole factor driving rotenone-induced cell death in these cells. This prompted us to perform an in-depth analysis of the underlying mechanism leading to rotenone-induced cell death.

Rotenone-induced cell death is accompanied by early mitochondrial dysfunction, increased ROS accumulation and defective autophagy

Since rotenone is a mitochondrial complex I inhibitor, the status of mitochondrial health following rotenone treatment was evaluated in both HEK293 and SH-SY5Y cells. Our results indicated that mitochondrial membrane depolarization started as early as 4 h post rotenone treatment (Fig. 2A, B). Further, we observed a significant loss in mitochondrial puncta structure (Fig. 2C, D) in SH-SY5Y and HEK293 cells along with an

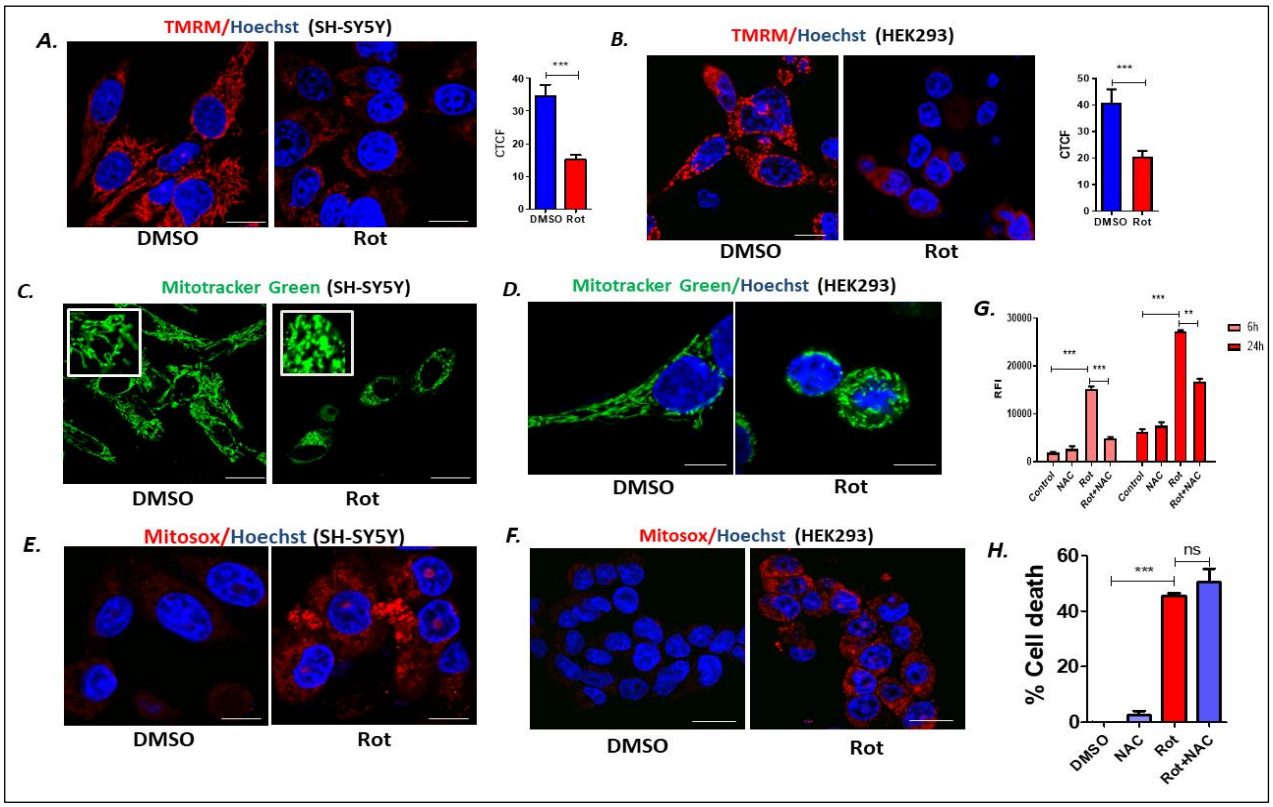

Fig. 2. Representative confocal images of SH-SY5Y and HEj293 cells stained with **(A- B)** TMRM. Right panel indicates the CTCF value **(C-D)** mitotracker green and **(E, F)** Mitosox red at 4 h post rotenone treatment. **(G-H)** Total cellular ROS production by using H2DCFDA and cell death by MTT assay were measured in NAC pre-incubated SH-SY5Y cells at the indicated time points.

heightened production of mitochondrial ROS (Fig. 2E, F) as determined by Mitosox staining. Pre-incubation of cells with the anti-oxidant N-acetyl cystine (NAC) significantly reduced ROS generation at both 6 h and 24 h post rotenone treatment (Fig. 2G) but did not reverse ongoing cell death process in these cells (Fig. 2H). Taken together, these data indicated that heightened ROS production may be the effect of accumulation of damaged mitochondria and may trigger a sequence of events that cannot be abrogated by prior treatment with NAC.

Accumulation of damaged mitochondria that resulted in heightened ROS production could be due to a defective mitochondrial turnover by autophagy. Therefore, to correlate mitochondrial dysfunction and increased ROS production we were inclined to check the status of autophagy in these cells following rotenone treatment. Our results showed an increase in p62 accumulation along with a reduction in Beclin-1 protein levels following rotenone treatment in SH-SY5Y cells [31] (Fig. 3A). To analyse the status of autophagosome formation, SH-SY5Y cells were transfected with GFP-LC3 and co-stained with p62, immunofluorescence analysis revealed that there was increased co-localization of GFP-LC3 with p62 indicating the formation of autophagosome (Fig. 3B). Next, we sought to determine whether p62 accumulation following rotenone treatment was due to decreased autophagosome-lysosome fusion or a defect in autophagic flux. For this, HEK293 cells were transfected with mCherry-EGFP-LC3B plasmid and since the EGFP signal is lost under the acidic pH of lysosome mCherry positive cells confirms a functional autophagic flux within the cells [32]. Our data suggests increased yellow puncta of LC3 in rotenone treated cells as opposed to the red puncta which indicated that a reduced autophagic flux could result in a limited turn-over of mitochondria in rotenone treated cells (Fig. 3C). Real-time analysis of key autophagy genes revealed a several fold higher expressions of early autophagy genes as compared to the DMSO-control cells but reduced expression of late Atg genes (Fig. 3D, E).

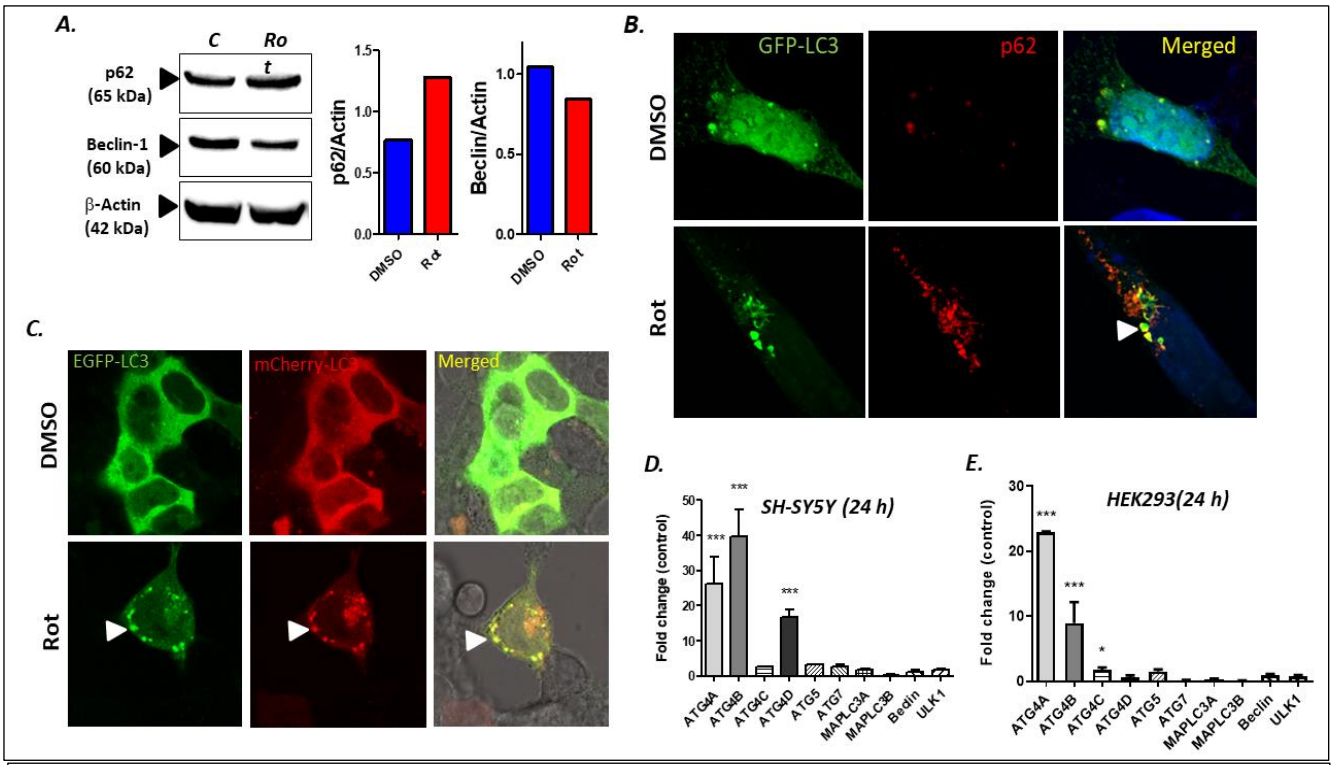

Fig. 3. (A) Immunoblot analysis of p62, Beclin1 proteins in SH-SY5Y cells treated with rotenone. B-actin served as a loading control. **(B)** Representative confocal images of SH-SY5Y cells transfected with GFP-LC3B and co-stained p62 and DAPI, 24 h post rotenone treatment. **(C)** HEK293 cells transfected with pbebe-EGFP-mCherry plasmid for 24 h followed by rotenone treatment. **(D, E)** RT-PCR analysis of Atg genes in both cell lines.

Rotenone treatment resulted in depletion of cellular NAD^+ levels and PARP inhibition by PJ34 prevented rotenone-induced cell death in both SH-SY5Y and HEK293 cells

Since, rotenone induced autophagy did not go to completion, we asked whether overall energy deficits within the cells prevented the autophagic degradation of damaged mitochondria. NAD^+ homeostasis has been shown to be intricately connected to a functional autophagy that may help the cells to adapt to energy deprived condition[33]. Our results suggested a significant decline in the NAD^+/NADH ratio following rotenone treatment (Fig. 4A). The reduction in NAD^+ levels prompted us to investigate whether the NAD^+ consuming enzymes like PARP1 and SIRT1 have any role in rotenone-induced cell death. To confirm our hypothesis, cells were pre-incubated with the PARP1 inhibitor PJ34 and we observed a significant reversal in rotenone-induced cell death at 24 h post treatment in SH-SY5Y cells (Fig. 4B, C). To confirm the importance of NAD^+ replenishment we quantified the NAD^+/NADH ratio and NAD^+ content at indicated time points in presence of PJ34 that showed reversal in the levels of NAD^+ in cells treated with rotenone in the presence of PJ34 (Fig. 4D, E). In comparison to the PARP inhibitor, the Sirtuin1 inhibitor EX527 had no such effect on rotenone mediated cell death (Fig. 4F). To determine whether PJ34 had a similar effect on other inhibitors of mitochondrial OXPHOS, cells were treated with the complex III inhibitor Antimycin and complex V inhibitor Oligomycin at the indicated doses. Our results suggested that PJ34 was unable to reverse the cell death induced by either Antimycin or Oligomycin (Fig. 4G-J) strongly suggesting that PARP1 inhibition specifically ameliorated rotenone-induced cell death.

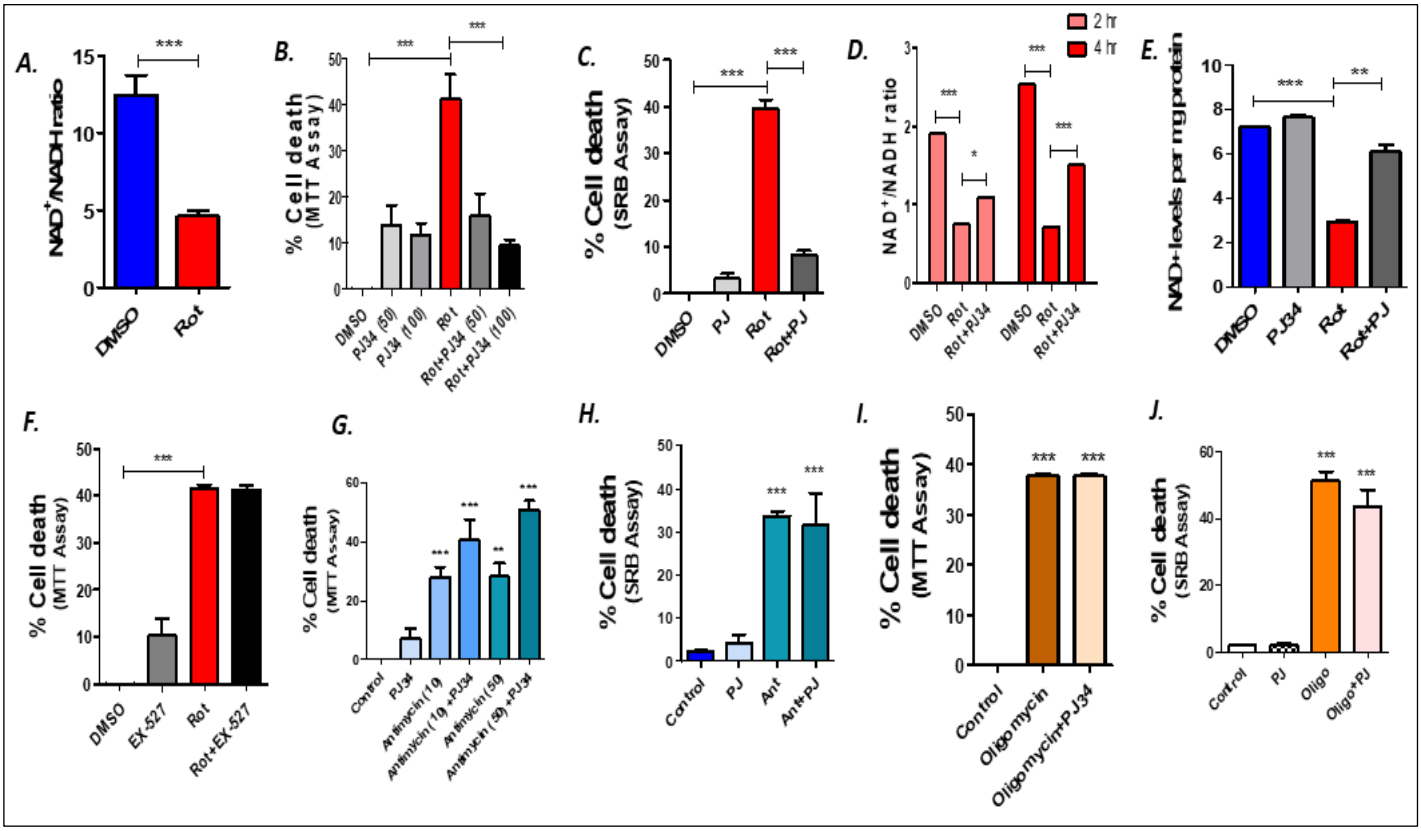

Fig. 4. (A) Quantitative analysis of NAD^+/NADH ratio in SH-SY5Y cells at 24 h post rotenone treatment. **(B-C)** Cell death measurement by MTT and SRB assay in SH-SY5Y cells pre-incubated with PJ34. **(D-E)** Quantitation of NAD^+/NADH ratio and measurement of total NAD^+ levels in the presence and absence of PJ34. **(F)** MTT assay performed in EX-527 (25µM) pre-incubated cells. **(G-H)** MTT assay **(I-J)** SRB assay following antimycin and oligomycin treatment in SH-SY5Y cells in the presence or absence of PJ34.

We hypothesized that the early drop in the NAD^+ levels were due to PARP hyperactivation due to DNA damage induced by accumulating ROS in the presence of rotenone. To test this further, we evaluated the protein levels of the DNA damage marker, phosphorylated H2AX, a histone marker of DNA double stand

break[34], the levels of which was upregulated in the presence of rotenone but reduced in the presence of PJ34 (Fig. 5A). To confirm PARP hyperactivation, the levels of poly-(ADP) ribose (PAR) was analysed and we noted a significant elevation in PAR levels following rotenone treatment in SH-SY5Y cells and pre-incubation with PJ34 reduced the PARylation (Fig. 5B). Further, a time dependent analysis of PAR protein levels showed a higher level of PAR at 4 h post-rotenone treatment in line with the previous observations (Fig. 5C). To further confirm the direct involvement of PARP1 in rotenone induced cell death, SH-SY5Y cells were transfected with siPARP1 (Fig. 5D) and cell death assays were performed and similar results were obtained as in case of PJ34 treated cells (Fig 5E). Taken together, these results pointed towards the importance of PARP1 inhibition in preventing rapid NAD^+ loss in rotenone mediated cell death.

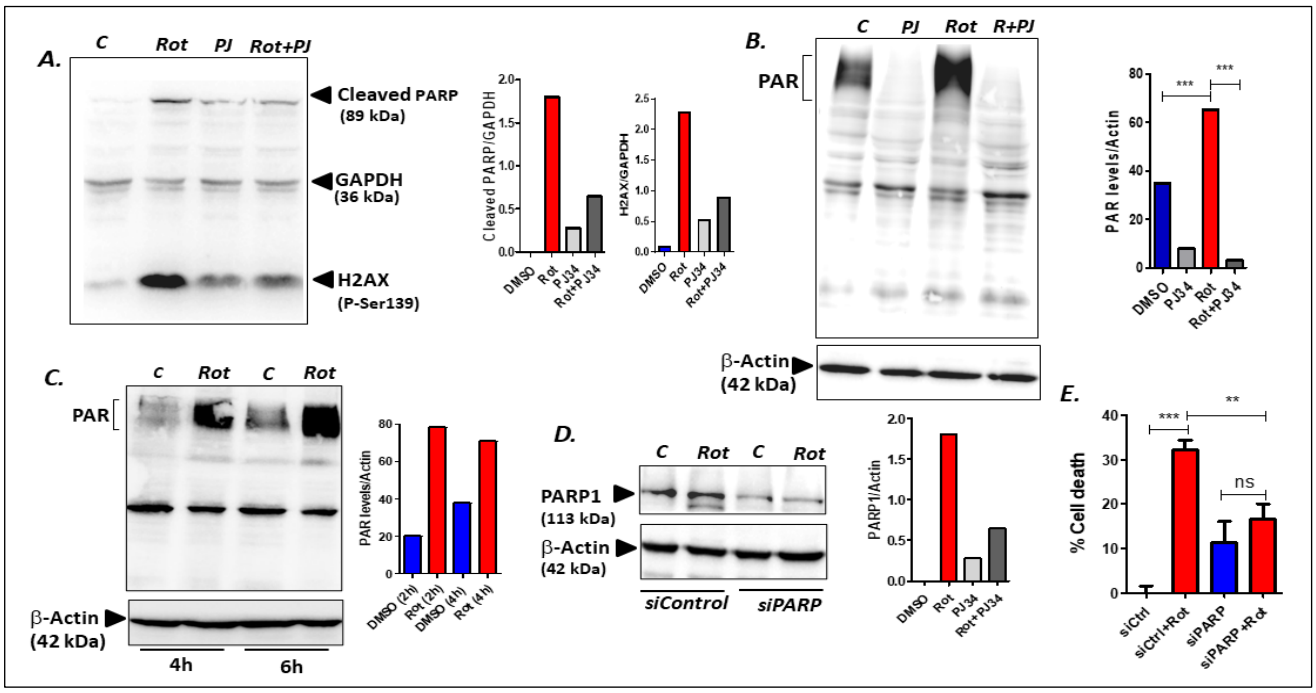

Fig. 5. (A) Immunoblot analysis of cleaved PARP, H2AX and GAPDH in SH-SY5Y cells treated with rotenone in the presence or absence of PJ34 **(B)** Immunoblot analysis of PARylation levels after indicated treatments. **(C)** Time dependent analysis of PARylation in SH-SY5Y cells following rotenone treatment. **(D)** Immunoblot analysis of siPARP transfected SH-SY5Y cells. **(E)** MTT assay was performed to quantify the percentage of cell death in PARP1 knock down SH-SY5Y cells.

Prior incubation of cells with the PARP inhibitor PJ-34 prevented the activation of the NADase Sarm1

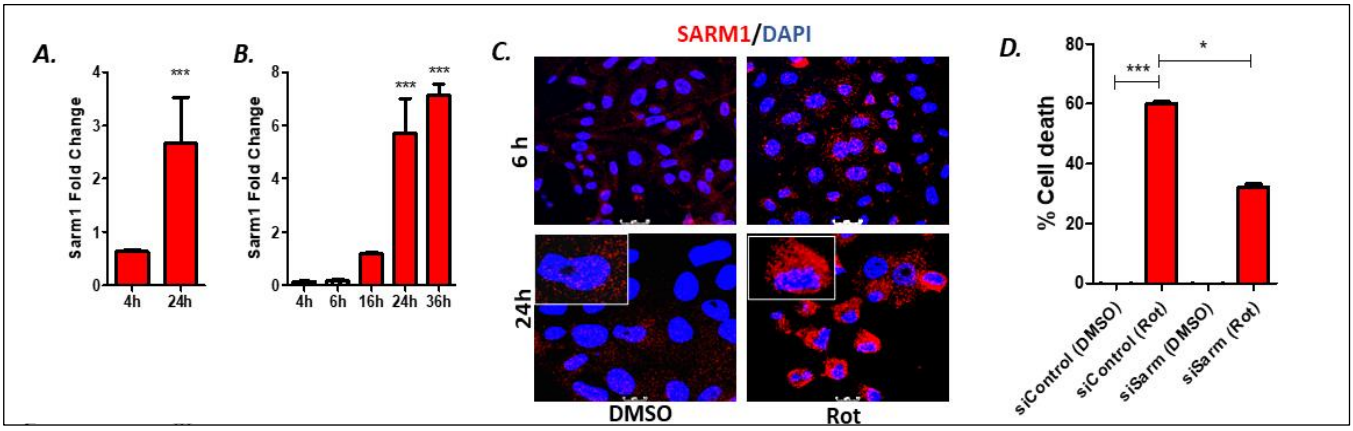

Fig. 6. (A, B) Time dependent quantification of SARM1 mRNA expression in HEK293 and SH-SY5Y cells. **(C)** Immunofluorescence analysis of SH-SY5Y cells probed with anti-SARM1 and DAPI at 4 h and 24 h post-rotenone treatment. **(D)** Cell death analysis in siSarm1 knock out HEK293 cells.

Our previous report suggested that the NADase Sarm1 is essential for rotenone-induced cell death in SH-SY5Y cells but the detailed mechanism remained elusive[35]. Here we observed increased *Sarm1* expression at 24 h post-rotenone treatment in both HEK293 and SH-SY5Y cells (Fig. 6A and B) but there was no induction of Sarm1 at the earlier time points indicating that mitochondrial dysfunction and deregulation of autophagy machinery occurred prior to Sarm1 induction in these cells. Additionally, we observed significantly higher levels of Sarm1 protein 24 h post-rotenone treatment in SH-SY5Y cells (Fig. 6C) *Sarm1* knock down by siRNA in HEK293 cells partially reversed rotenone-induced cell death (Fig 6D) indicating activation of Sarm1 might lead to further decline in NAD^+ levels thus promoting cell death.

Interestingly, PJ34 pre-incubation prominently reduced the mRNA expression of *Sarm1* following rotenone treatment (Fig. 7A) as well as Sarm1 activity as determined by the cADPR levels, a by-product of Sarm1 activation[36] (Fig. 7B). Since, Sarm1 stabilizes on depolarised mitochondria[37], we proceeded to check the

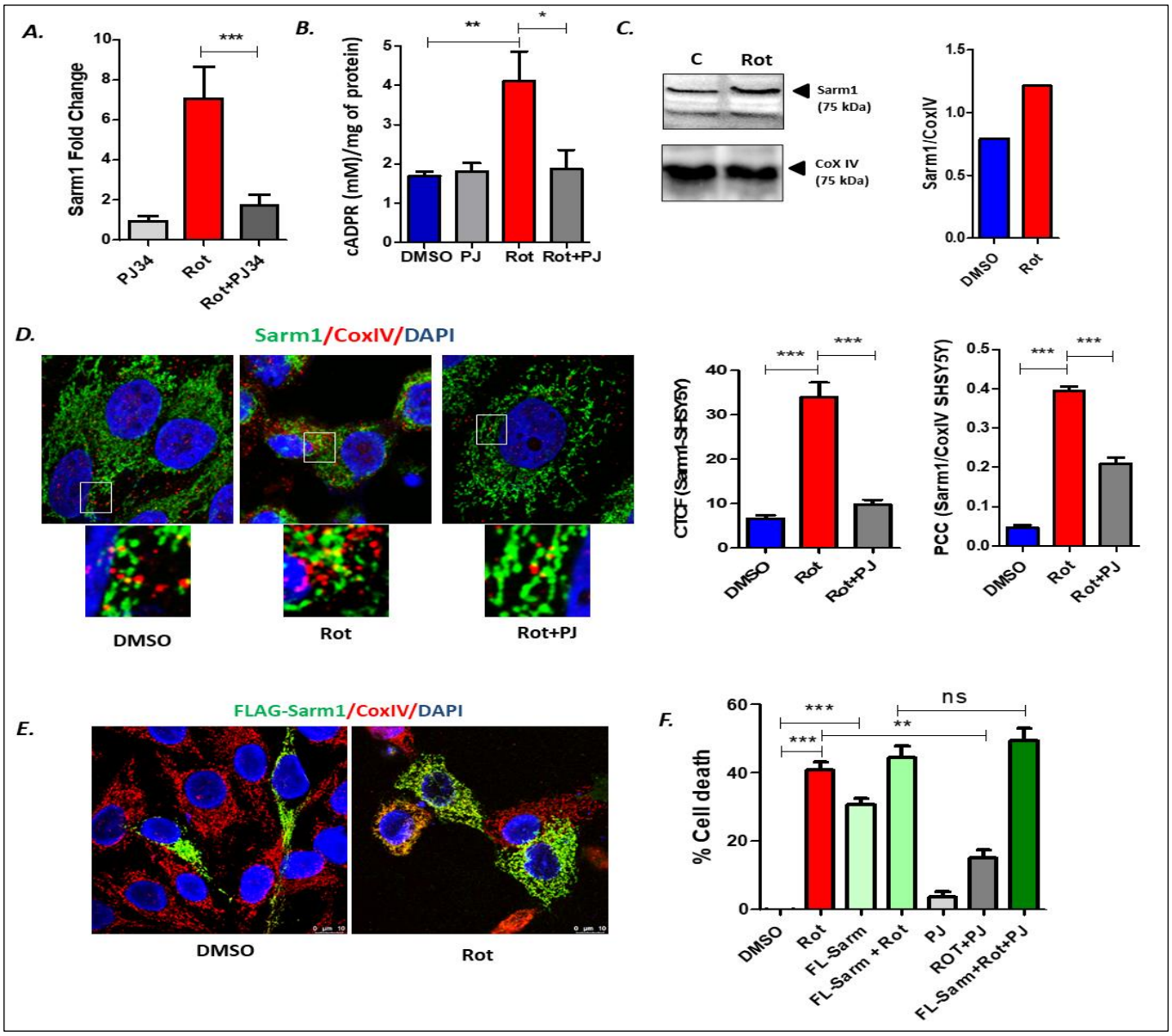

Fig. 7. (A) Relative mRNA expression of SARM quantified by fold change method in presence of PJ-34 followed by rotenone treatment. **(B)** The level of cADPR at 24 h post treatment. **(C)** Western blot analysis of Sarm1 in mitochondrial fraction, COXIV served as a mitochondrial marker. **(D)** Representative confocal images of Sarm1 with mitochondrial marker protein COXIV 24 h post treatment (left panel). Representation of CTCF values and Pearsons' co-efficient for colocalization analysis (right panel). **(E)** FLAG-Sarm1 overexpression in SH-SY5Y cells followed by cell death analysis **(F)** at 24 h post treatment.

localization of Sarm1 at mitochondria and found increased levels of Sarm1 protein in mitochondrial fraction 24 h post-rotenone treatment (Fig. 7C) and this mitochondrial localization was reduced in presence of PJ34 (Fig. 7D). To understand the importance of the temporal induction of Sarm1 as observed in both HEK293 and SH-SY5Y cells, we asked whether PJ34 could still be functional in preventing rotenone-induced cell death in cells overexpressing Sarm1 (Fig. 7E). Interestingly, our data suggests that in contrast to the un-transfected cells, PJ34 could not reverse rotenone induced cell death in Sarm1-overexpressed cells (Fig. 7F) which point towards the importance of the early events leading up to Sarm1 activation that may act as the final trigger of cell death.

PJ-34 restored mitochondrial homeostasis and prevented the accumulation of damaged mitochondria upon rotenone treatment

Since, we hypothesized that rotenone-induced mitochondrial damage led to ROS production and DNA damage induced hyperactivation of PARP1 followed by Sarm1 activation and cell death, we assessed the status of mitochondria following PARP inhibition. Our result suggested that pre-incubation of cells with PJ34 significantly reduced the mitochondrial ROS production along with total cellular ROS levels as indicated by Mitosox staining and H2DCFDA assay (Fig. 8A, B). The mitochondrial membrane potential was also restored in PJ34 treated SH-SY5Y cells (Fig. 8C).

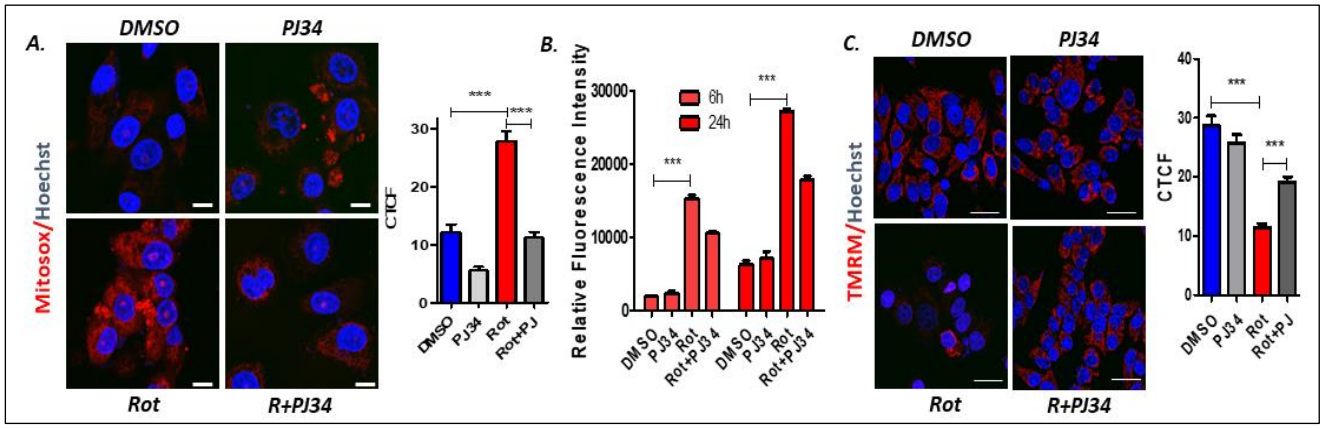

Fig. 8. (A) Representative confocal images of SH-SY5Y cells stained with mitosox red and Hoechst 4 h post treatment. **(B)** The total cellular ROS levels was measured by H2DCFDA assay. **(C)** SH-SY5Y cells stained with TMRM to assess the mitochondrial membrane potential at 4 h post treatment.

To understand the status of respiratory complex activity, mitochondrial complex I activity was quantified in these cells and a significant restoration of Complex I activity was observed in PJ34 treated cells (Fig. 9A, B) along with moderate restoration of ATP levels (Fig. 9C) and increased protein level of ATP5A (Fig. 9D).

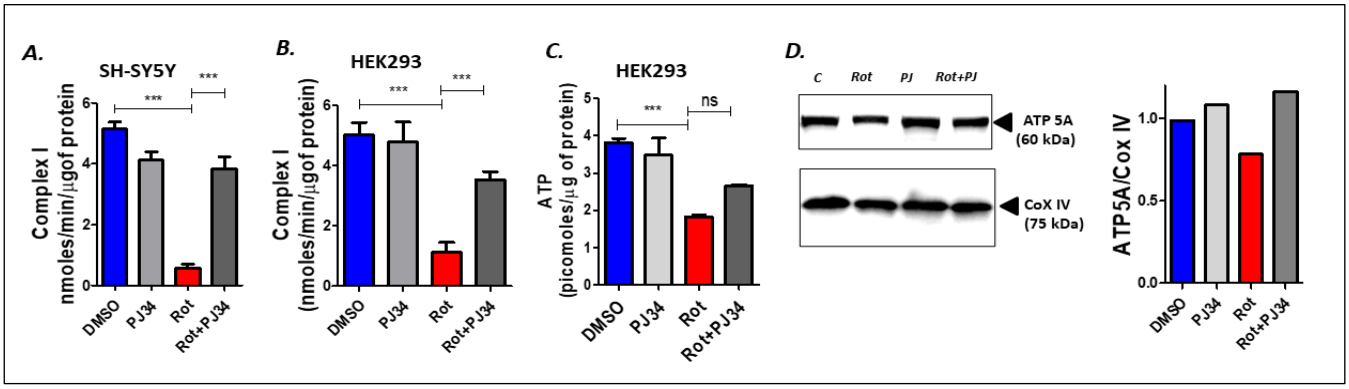

Fig. 9. (A-B) The activity of mitochondrial complex I was measured in HEK293 and SH-SY5Y cells and results were expressed as units/microgram of protein. **(C)** ATP levels were determined 24 h post treatment. **(D)** Immunoblot analysis of mitochondrial respiratory chain protein ATP5A. COXIV served as an internal marker of mitochondrial fraction. The right panel representing the densitometric analysis of the immunoblot.

To understand the importance of mitochondrial turnover via autophagy in rotenone-induced cell death, SH-SY5Y cells were transfected with a traffic light mitophagy reporter mito-mRFP-EGFP plasmid [38]. The red fluorescence is indicative of mitophagy as the EGFP signal will be lost under acidic pH of lysosome. Our results indicated increased mitophagy at localised site within the cells treated with rotenone in presence of PJ34 as compared to rotenone alone (Fig. 10A). To further confirm the role of autophagy in mitochondrial homeostasis, cells were pre-incubated with autophagy inhibitor chloroquine (CQ) in presence and absence of rotenone and PJ34. The results indicated a higher mitotracker to lysotracker co-localisation in PJ34 incubated cells compared to CQ and no reversal of cell death was observed in the presence of CQ which indicated that a functional autophagy is required for PJ34 mediated cell death reversal (Fig. 10B, C). In line with these observations, we sought to determine the role of Sirt1 as it has a positive regulatory role in autophagy in an NAD^+ dependent manner[39]. It may be noted here that cells lacking SIRT1 had a significantly higher amount of cell death than the siControl cells. Knockdown of SIRT1 was confirmed in these cells by immunostaining with SIRT1 antibody (Fig. 10E). Collectively, these results suggest that a functional autophagy is probably linked with cell death in rotenone treated cells that can be alleviated by PJ34 by restoring cellular NAD^+ levels and cannot be achieved by stimulating autophagy alone.

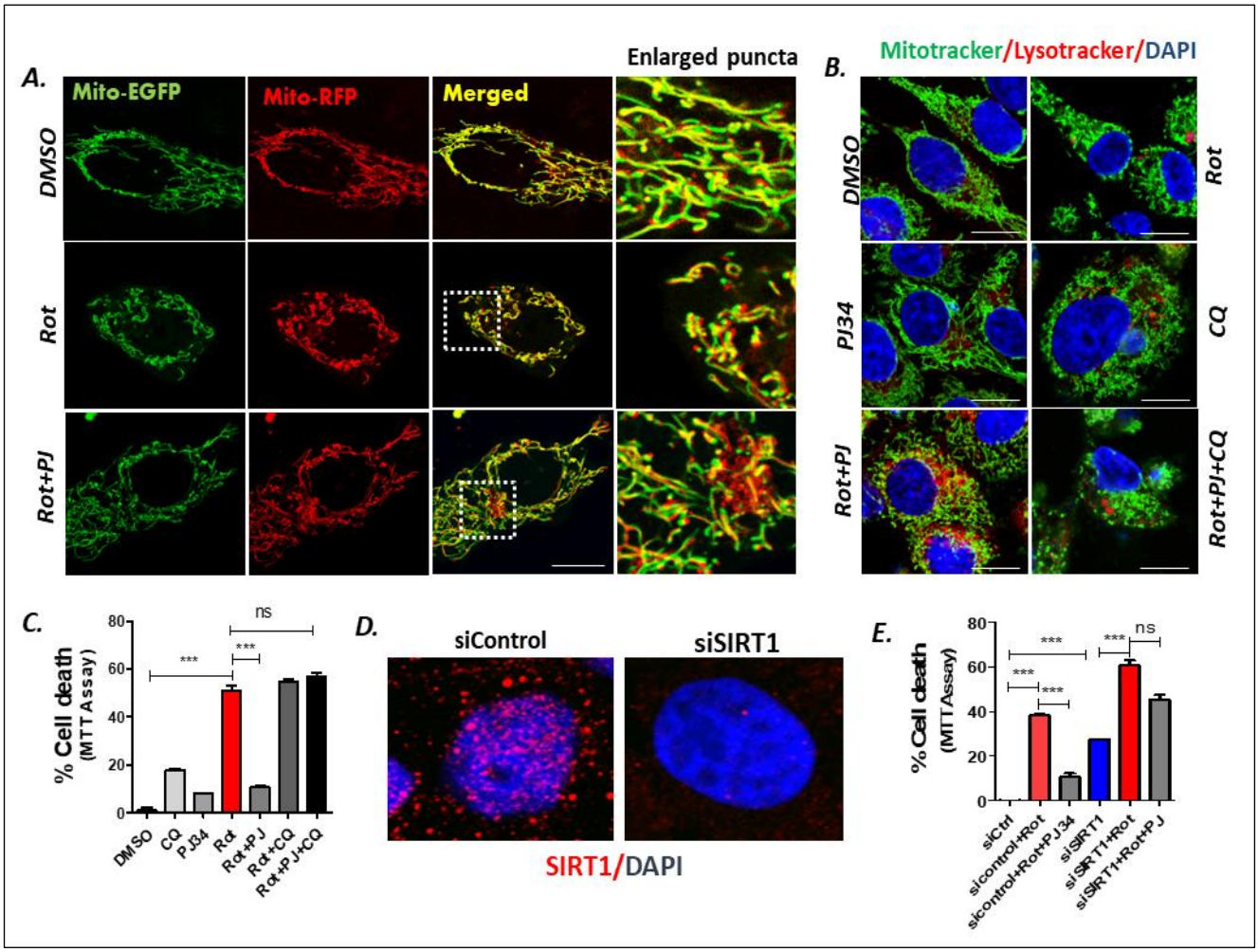

Fig. 10. (A) Mitophagy assay in SH-SY5Y cells transfected with mito-EGFP-RFP for 24 h followed by indicated treatments. **(B)** Confocal images of SH-SY5Y cells pre-incubated with autophagy inhibitor chloroquine (50μM) and co-stained with mitotracker and lysotracker 24 h post treatment. **(C)** Percentage of cell death in presence of chloroquine along with rotenone and PJ34. **(D)** Confocal images of *SIRT1* knock down in SH-SY5Y cells. **(E)** Quantification of cell death by MTT assay in SIRT1 known down SH-SY5Y cells at 24 h in the presence or absence of rotenone.

Objective II: Repurposing PARP1 inhibitors as therapeutic strategy in the context of neurodegenerative diseases

The aim of this objective is to establish the molecular mechanism in an *in-vivo* model system to understand whether PARP inhibitor can be repurposed for neuroprotection.

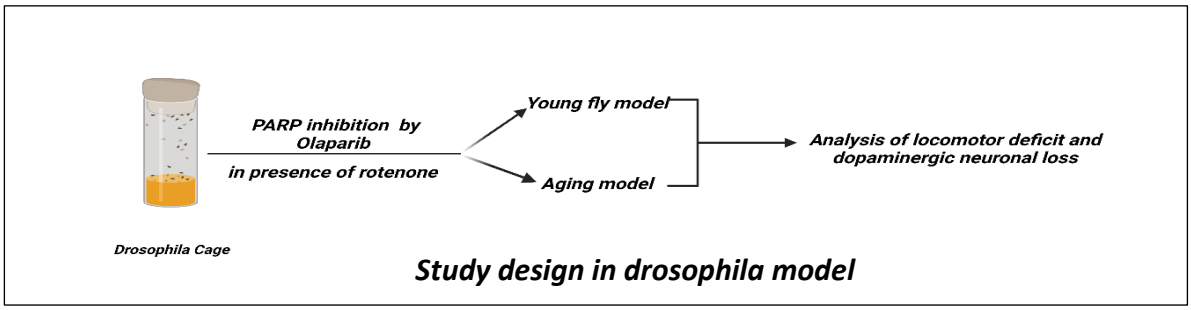
PARP inhibition by Olaparib
in presence of rotenone
Young fly model
Aging model
Analysis of locomotor deficit and dopaminergic neuronal loss
Drosophila Cage
Study design in drosophila model

The PARP inhibitor Olaparib prevents rotenone-induced neurodegeneration and locomotor deficits

To strengthen our understanding on the effect of PARP inhibition, we extended our studies with the PARP inhibitor Olaparib which is a clinically approved catalytic inhibitor of PARP1 and known for its neuroprotective role in AD[40,41, 42]. Our results revealed that a dose of 50 µM induced around 30% cell death in these cells. Hence, we chose a sub-optimal dose of 20 µM to study the effect of Olaparib on rotenone induced cell death (Fig. 11A). Pre-incubation of cells with Olaparib followed by rotenone treatment significantly reversed rotenone induced cell death in SH-SY5Y cells at 24h post treatment (Fig. 11B).

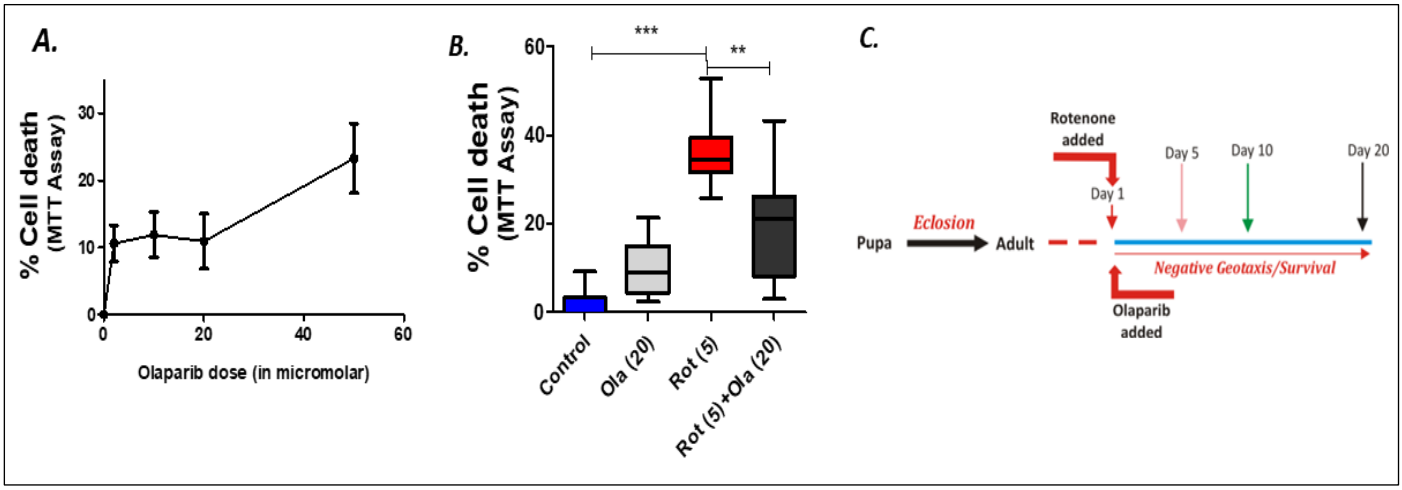

Fig. 11. (A) Olaparib dose standardization in SH-SY5Y cells. **(B)** Percentage of cell death calculation by MTT assay 24 h post treatment in SH-SY5Y cells. **(C)** Experimental strategy in drosophila model of young flies.

To further understand the physiological relevance of PARP inhibition by Olaparib in rotenone induced pathological condition, we extended our data in fruit fly *Drosophila melanogaster*. Olaparib has shown promising effect as an anti-cancer chemotherapeutic drug and is sold under the trade name Lynparza to treat ovarian cancer[43]. Due to its known prospect in drug repurposing, we selected Olaparib for PARP inhibition instead of PJ34 in our studies. For this, w^{1118} flies were exposed in presence or absence of Olaparib at indicated doses at different time points (Fig. 11C).

Interestingly, exposure to Olaparib reversed rotenone induced locomotor deficit in 1-day old flies incubated with the drugs for 5-, 10- and 20-days respectively (Fig. 12A-C). This reversal in locomotor ability was accompanied by a significant decrease in the levels of pro-neurodegenerative molecule Ect4 levels (dSARM) (Fig 12D). The increase in dSarm correlated with the NAD^+/NADH ratio that clearly indicated a decline in NAD^+ levels following rotenone treatment (Fig. 12E) indicating that the NADase dSARM may

play a role in the neurodegenerative processes during rotenone exposure in the flies. To check the effect of Olaparib on fly survival, percentage of survival was calculated and represented for each set of flies receiving different treatment (Fig. 12F and G).

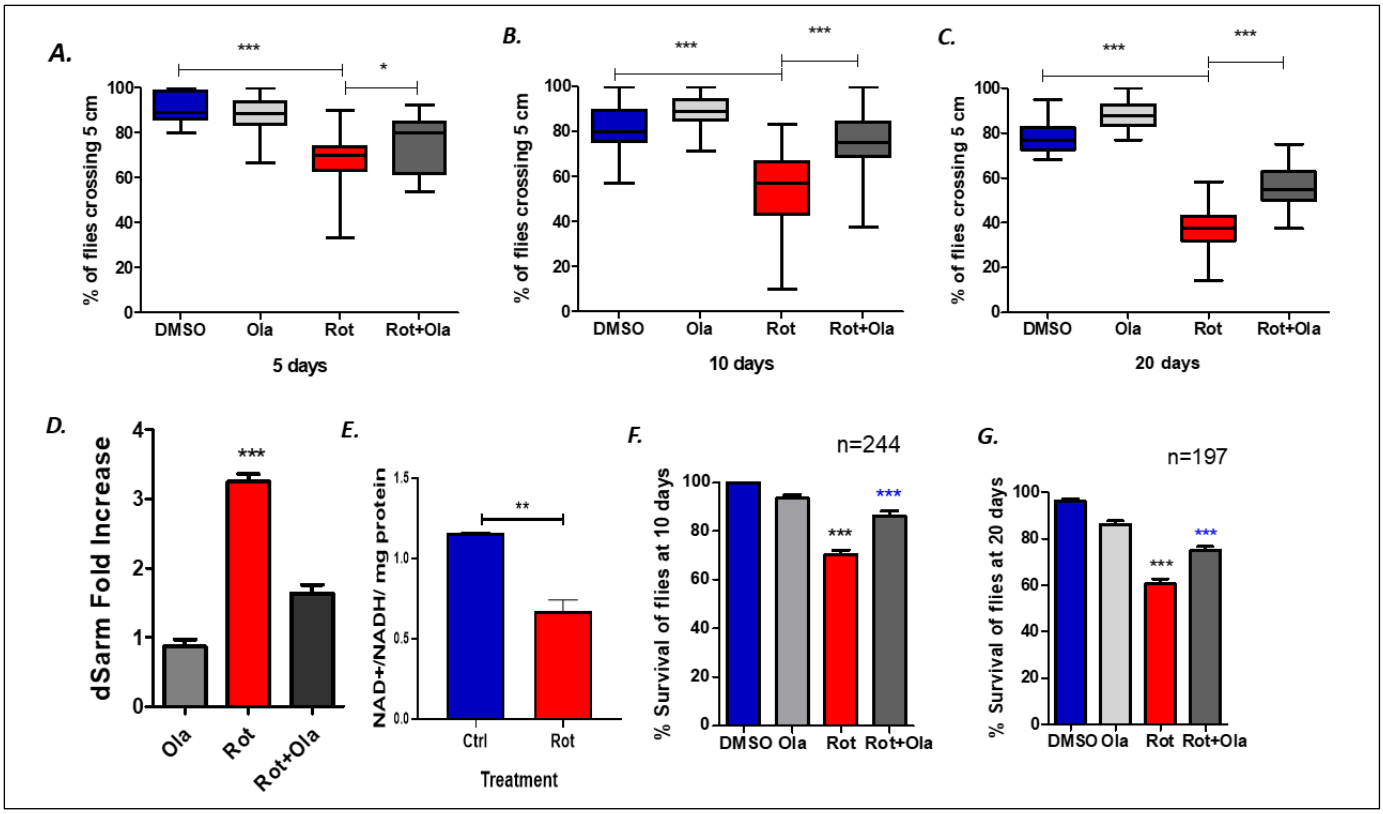

Fig. 12. (A-C) Determination of locomotor ability by negative geotaxis assay in 5-days, 10-days, and 20-days old flies incubated with indicated drugs. **(D)** Quantitative analysis of mRNA expression of dSarm following rotenone exposure of flies in the presence or absence of Olaparib. **(E)** Determination of NAD^+ levels post rotenone treatment in 20-days old flies. **(F-G)** Percent survival of flies following exposure to rotenone in the presence or absence of Olaparib for 10-days and 20-days.

Pre-incubation of w^{1118} flies with Olaparib prevents rotenone induced locomotor deficits in aging flies

We have previously, shown that aged flies are more susceptible to rotenone treatment compared to the young flies due to increased expression of *dSarm1* [35]. Here, we asked whether prior exposure to Olaparib could reverse the locomotor deficits following rotenone treatment in the aging flies as well. To confirm this phenomenon, we pre-incubated the 1-day old flies in standard media and 100 µM Olaparib containing media for up to 20 days, the strategy for which is depicted in Fig. 13A. After 20 days of incubation period, the flies were transferred to rotenone containing media for 3-days and 5-days. The locomotor ability of the flies was determined by conducting climbing assay and the observations were compared with the control samples (Fig. 13B-E). Our data suggested a significant reversal of locomotor ability in the aging flies that were exposed to Olaparib prior to rotenone treatment. This is the first study showing such a reversal of locmotor deficits following PARP inhibition and paves the way for further exploration for therapeutic intervention in environmental toxin induced neurodegeneration.

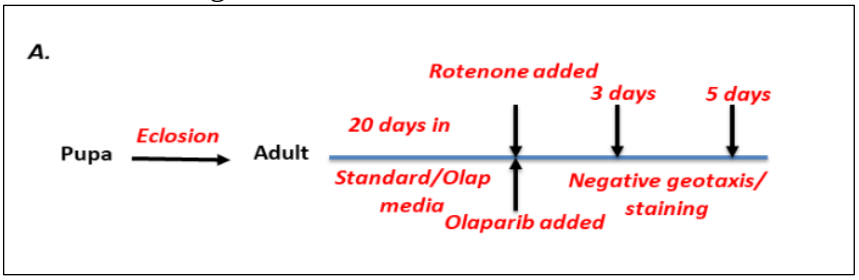

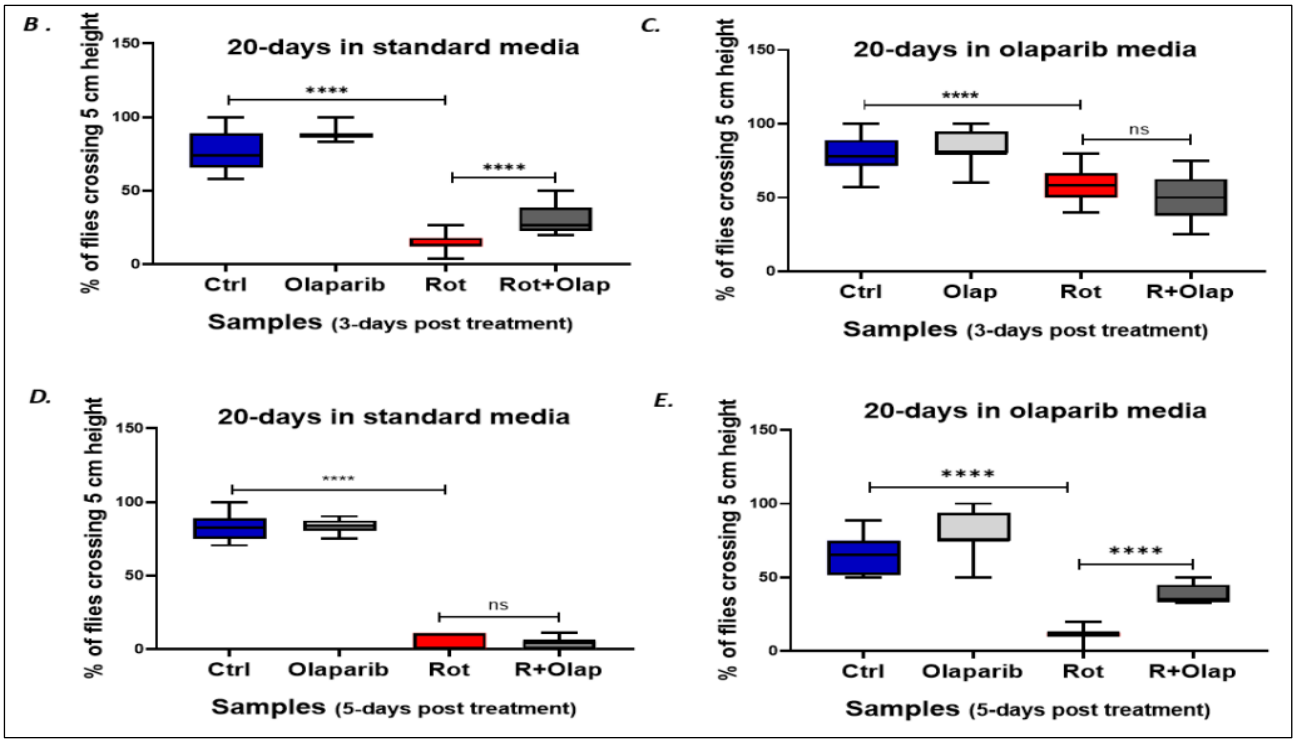

Fig. 13. (A) Schematic representation of experimental setup with olaprib in 20-day old flies **(B-C)** Determination of locomotor ability by negative geotaxis assay in 20-days old flies incubated in standard media (C) and Olaparib containing media (D) followed by 3-days of treatment. **(D-E)** Determination of locomotor ability by negative geotaxis assay in 20-days old flies incubated in standard media (C) and Olaparib containing media (D) followed by 5-days of treatment.

Pre-incubation with Olaparib prevents the loss of dopaminergic neurons in response to rotenone treatment

The high energy demands of dopaminergic neurons (DA) in the par compacta region of the brain due to their anatomical structure and tonic activity renders these neurons vulnerable to degeneration[44]. Degeneration of these neurons are hallmark of Parkinson's disease. To understand the effect of PARP inhibition on the survivability of the dopaminergic (DA) neurons, the fly brains were immuno-stained with DA specific marker Tyrosine hydroxylase (TH) to analyze the DA neuronal clusters. We observed a greater number of DA neuronal clusters in Olaparib pre-incubated flies that were comparable to control samples (Fig. 14 B) but in case of the flies fed with rotenone alone, there was increased degeneration of DA neuronal clusters (Fig. 14 A, B). However, aging flies exposed to Olaparib along with rotenone at 20-days showed no signs of reversal of DA neuronal loss (Fig. 14 A). Taken together, these observations indicated that PARP1 inhibition could reverse the hallmarks of aging in flies like survivability, locomotor deficits and loss of DA neurons following exposure to rotenone that could open up exciting opportunities in the treatment of neurodegenerative diseases like sporadic forms of PD.

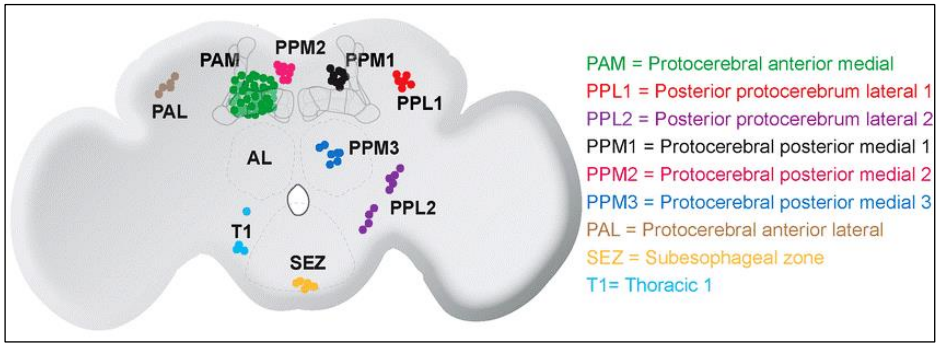

Representative diagram of dopaminergic neuronal clusters in *Drosophila melanogaster* brain

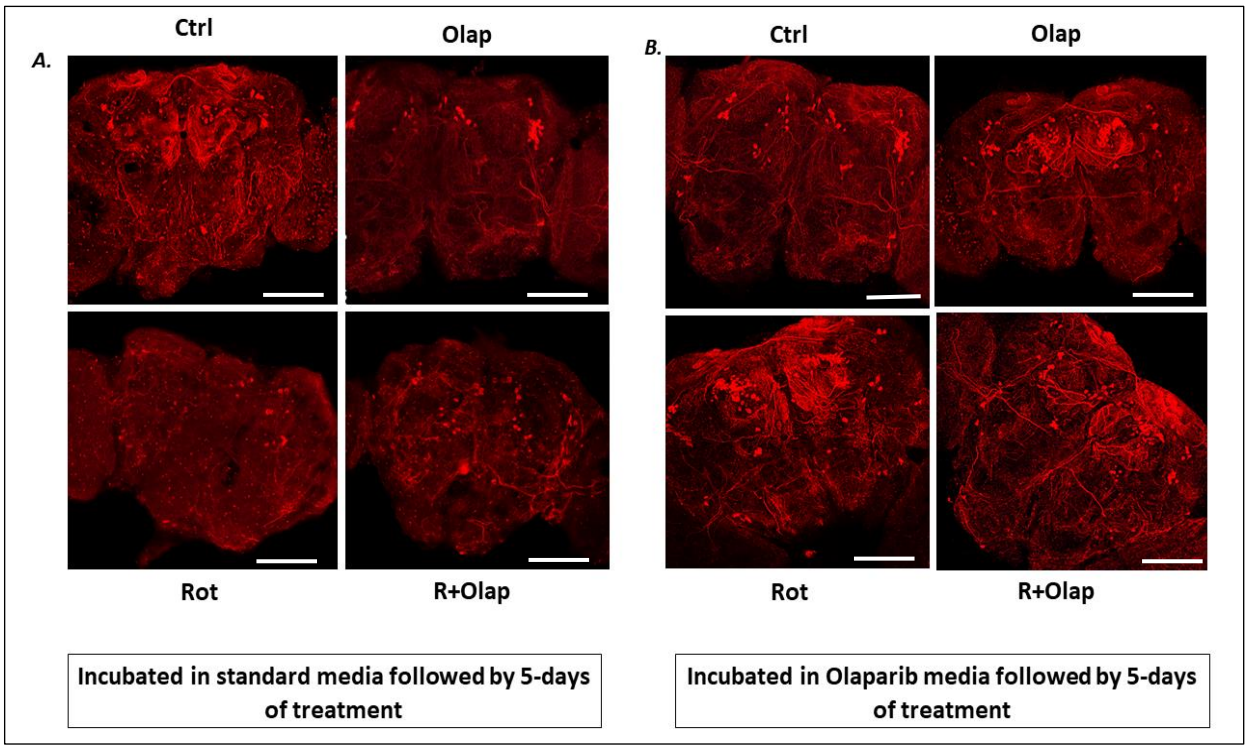

Fig. 14. Representative confocal images of drosophila brain stained with anti-TH to analyse the dopaminergic neuronal clusters at 5-days post-rotenone treatment in the presence or absence of Olaparib. In panel **(A)** flies were incubated in standard media for 20 days followed by 5-days of treatment. **(B)** Flies were pre-incubated in Olaparib media for 20 day followed by 5-days of treatment in the presence or absence of rotenone.

Conclusion:

This is the first study describing the temporal regulation of NAD^+ consuming enzymes in response to mitochondrial complex I inhibition following rotenone treatment. The research study includes both *in-vitro* and *in-vivo* models that demonstrates that PARP1 mediated early loss of NAD^+ is involved in the activation and mitochondrial translocation of NADase Sarm1. We also show that the NAD^+ loss results in a defect in mitophagy resulting in the accumulation of damaged mitochondria that could be ameliorated by PARP inhibition. The *in-vivo* analysis in *Drosophila* provides a novel idea of repurposing of PARP inhibitors as a neuroprotective agent, the proposed mechanism of which depicted in the model (Fig. 15).

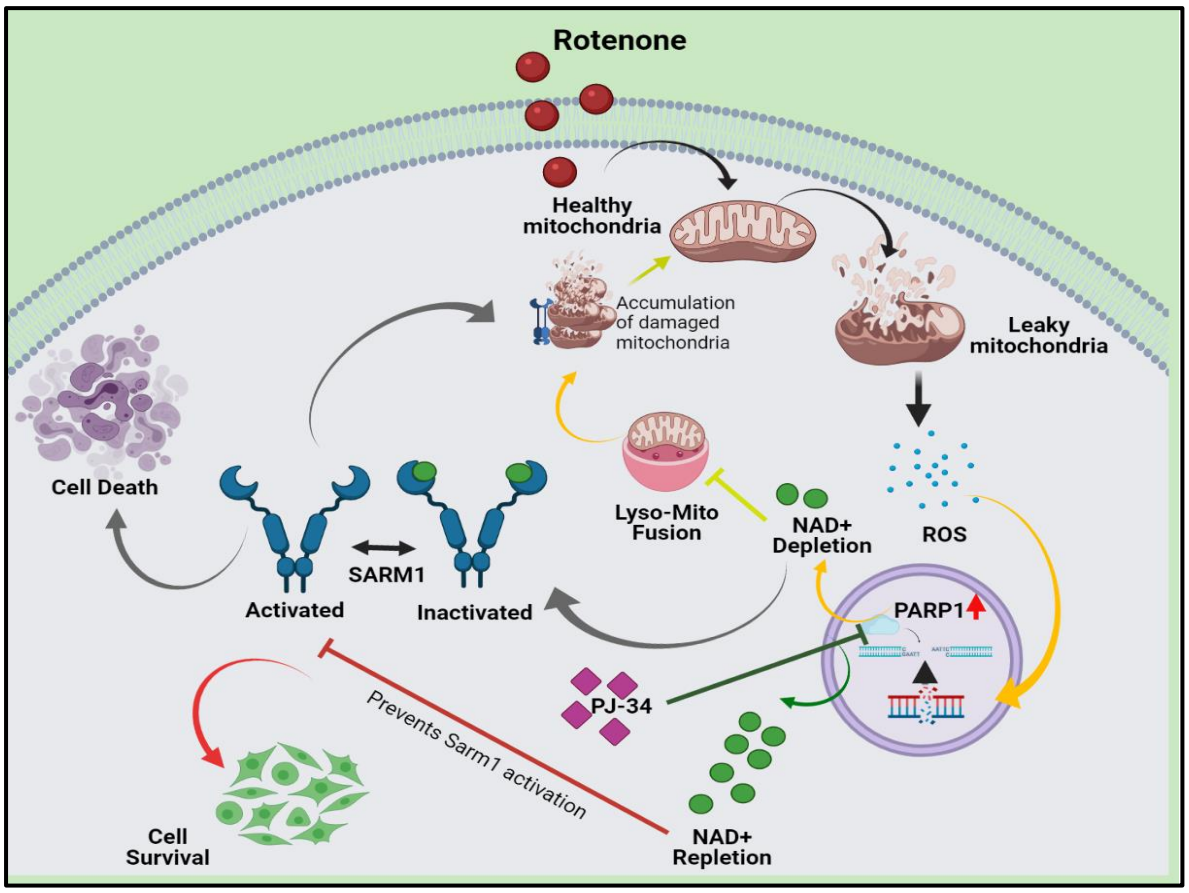

Fig. 15. Schematic Representation of the mechanistic regulation of rotenone induced mitochondrial dysregulation and its interconnection with NAD^+ metabolism.

References:

1. Berthiaume, J. M., Kurdys, J. G., Muntean, D. M. & Rosca, M. G. Mitochondrial NAD + /NADH redox state and diabetic cardiomyopathy. *Antioxidants and Redox Signaling* vol. 30 375–398 Preprint at https://doi.org/10.1089/ars.2017.7415 (2019).

2. Huang, X. *et al.* NAD+ Modulates the Proliferation and Differentiation of Adult Neural Stem/Progenitor Cells via Akt Signaling Pathway. *Cells* **11**, (2022).

3. Zapata-Pérez, R., Wanders, R. J. A., Karnebeek, C. D. M. & Houtkooper, R. H. NAD + homeostasis in human health and disease. *EMBO Mol Med* **13**, (2021).

4. Nagro, C. del, Xiao, Y., Rangell, L., Reichelt, M. & O'Brien, T. Depletion of the Central Metabolite NAD leads to oncosismediated cell death. *Journal of Biological Chemistry* **289**, 35182–35192 (2014).

5. Lundt, S. & Ding, S. NAD+ metabolism and diseases with motor dysfunction. *Genes* vol. 12 Preprint at https://doi.org/10.3390/genes12111776 (2021).

6. Berthiaume, J. M., Kurdys, J. G., Muntean, D. M. & Rosca, M. G. Mitochondrial NAD + /NADH redox state and diabetic cardiomyopathy. *Antioxidants and Redox Signaling* vol. 30 375–398 Preprint at https://doi.org/10.1089/ars.2017.7415 (2019).

7. Murata, M. M. *et al.* NAD+ consumption by PARP1 in response to DNA damage triggers metabolic shift critical for damaged cell survival. *Mol Biol Cell* **30**, 2584–2597 (2019).

8. Cerutti, R. *et al. Supplemental Information NAD +-Dependent Activation of Sirt1 Corrects the Phenotype in a Mouse Model of Mitochondrial Disease*. *Cell Metabolism* vol. 19.

9. Summers, D. W., Gibson, D. A., DiAntonio, A. & Milbrandt, J. SARM1-specific motifs in the TIR domain enable NAD+ loss and regulate injury-induced SARM1 activation. *Proc Natl Acad Sci U S A* **113**, E6271–E6280 (2016).

10. Ko, H. L. & Ren, E. C. Functional aspects of PARP1 in DNA repair and transcription. *Biomolecules* vol. 2 524–548 Preprint at https://doi.org/10.3390/biom2040524 (2012).

11. Essuman, K. *et al.* The SARM1 Toll/Interleukin-1 Receptor Domain Possesses Intrinsic NAD+ Cleavage Activity that Promotes Pathological Axonal Degeneration. *Neuron* **93**, 1334-1343.e5 (2017).

12. Hariharan, N. *et al.* Deacetylation of FoxO by Sirt1 plays an essential role in mediating starvation-induced autophagy in cardiac myocytes. *Circ Res* **107**, 1470–1482 (2010).

13. Ray Chaudhuri, A. & Nussenzweig, A. The multifaceted roles of PARP1 in DNA repair and chromatin remodelling. *Nature Reviews Molecular Cell Biology* vol. 18 610–621 Preprint at https://doi.org/10.1038/nrm.2017.53 (2017).

14. Cohen, M. S. Interplay between compartmentalized NAD+ synthesis and consumption: A focus on the PARP family. *Genes and Development* vol. 34 254–262 Preprint at https://doi.org/10.1101/gad.335109.119 (2020).

15. Zhu, Y., Liu, J., Park, J., Rai, P. & Zhai, R. G. Subcellular compartmentalization of NAD+ and its role in cancer: A sereNADe of metabolic melodies. *Pharmacology and Therapeutics* vol. 200 27–41 Preprint at https://doi.org/10.1016/j.pharmthera.2019.04.002 (2019).

16. Castro-Portuguez, R. & Sutphin, G. L. Kynurenine pathway, NAD+ synthesis, and mitochondrial function: Targeting tryptophan metabolism to promote longevity and healthspan. *Experimental Gerontology* vol. 132 Preprint at https://doi.org/10.1016/j.exger.2020.110841 (2020).

17. 10. NAD+ metabolism_ Bioenergetics, signaling and manipulation for therapy _ Enhanced Reader.

18. Hanaford, A. & Johnson, S. C. The immune system as a driver of mitochondrial disease pathogenesis: a review of evidence. *Orphanet Journal of Rare Diseases* vol. 17 Preprint at https://doi.org/10.1186/s13023-022-02495-3 (2022).

19. Sharma #, L. K., Lu, J. & Bai, Y. *Mitochondrial Respiratory Complex I: Structure, Function and Implica-tion in Human Diseases*. *Current Medicinal Chemistry* vol. 16 (2009).

20. Sousa, F. G. *et al.* PARPs and the DNA damage response. *Carcinogenesis* vol. 33 1433–1440 Preprint at https://doi.org/10.1093/carcin/bgs132 (2012).

21. Hurtado-Bagès, S., Knobloch, G., Ladurner, A. G. & Buschbeck, M. The taming of PARP1 and its impact on NAD+ metabolism. *Molecular Metabolism* vol. 38 Preprint at https://doi.org/10.1016/j.molmet.2020.01.014 (2020).

22. Lu, P. *et al.* Poly (ADP-ribose) polymerase-1 inhibits mitochondrial respiration by suppressing PGC-1α activity in neurons. *Neuropharmacology* **160**, (2019).

23. Mashimo, M. *et al.* The 89-kDa PARP1 cleavage fragment serves as a cytoplasmic PAR carrier to induce AIF-mediated apoptosis. *Journal of Biological Chemistry* **296**, (2021).

24. Zha, S., Li, Z., Cao, Q., Wang, F. & Liu, F. PARP1 inhibitor (PJ34) improves the function of aging-induced endothelial progenitor cells by preserving intracellular NAD + levels and increasing SIRT1 activity. *Stem Cell Res Ther* **9**, (2018).

25. Robson, M. *et al.* Olaparib for Metastatic Breast Cancer in Patients with a Germline BRCA Mutation. *New England Journal of Medicine* **377**, 523–533 (2017).

26. Bai, P. & Cantó, C. The role of PARP-1 and PARP-2 enzymes in metabolic regulation and disease. *Cell Metabolism* vol. 16 290–295 Preprint at https://doi.org/10.1016/j.cmet.2012.06.016 (2012).

27. Bai, P. *et al.* PARP-1 inhibition increases mitochondrial metabolism through SIRT1 activation. *Cell Metab* **13**, 461–468 (2011).

28. Sporny, M. *et al.* Structural basis for sarm1 inhibition and activation under energetic stress. *Elife* **9**, 1–25 (2020).

29. Bratkowski, M. *et al.* Structural and Mechanistic Regulation of the Pro-degenerative NAD Hydrolase SARM1. *Cell Rep* **32**, (2020).

30. Radad, K., Rausch, W. D. & Gille, G. Rotenone induces cell death in primary dopaminergic culture by increasing ROS production and inhibiting mitochondrial respiration. *Neurochem Int* **49**, 379–386 (2006).

31. Pankiv, S. *et al.* p62/SQSTM1 binds directly to Atg8/LC3 to facilitate degradation of ubiquitinated protein aggregates by autophagy*[S]. *Journal of Biological Chemistry* **282**, 24131–24145 (2007).

32. Runwal, G. *et al.* LC3-positive structures are prominent in autophagy-deficient cells. *Sci Rep* **9**, (2019).

33. Fang, E. F. *et al.* NAD+ augmentation restores mitophagy and limits accelerated aging in Werner syndrome. *Nat Commun* **10**, (2019).

34. Mah, L. J., El-Osta, A. & Karagiannis, T. C. γh2AX: A sensitive molecular marker of DNA damage and repair. *Leukemia* vol. 24 679–686 Preprint at https://doi.org/10.1038/leu.2010.6 (2010).

35. Sur, M. *et al.* Sarm1 induction and accompanying inflammatory response mediates age-dependent susceptibility to rotenone-induced neurotoxicity. *Cell Death Discov* **4**, (2018).

36. Sasaki, Y. *et al.* cADPR is a gene dosage-sensitive biomarker of SARM1 activity in healthy, compromised, and degenerating axons. *Exp Neurol* **329**, (2020).

37. Murata, H., Sakaguchi, M., Kataoka, K. & Huh, N. H. SARM1 and TRAF6 bind to and stabilize PINK1 on depolarized mitochondria. *Mol Biol Cell* **24**, 2772–2784 (2013).

38. Kim, S. J. *et al.* Hepatitis B Virus Disrupts Mitochondrial Dynamics: Induces Fission and Mitophagy to Attenuate Apoptosis. *PLoS Pathog* **9**, 1–12 (2013).

39. Ou, X., Lee, M. R., Huang, X., Messina-Graham, S. & Broxmeyer, H. E. SIRT1 positively regulates autophagy and mitochondria function in embryonic stem cells under oxidative stress. *Stem Cells* **32**, 1183–1194 (2014).

40. Mao, K. & Zhang, G. The role of PARP1 in neurodegenerative diseases and aging. *FEBS Journal* vol. 289 2013–2024 Preprint at https://doi.org/10.1111/febs.15716 (2022).

41. Maggiore, A. *et al.* Neuroprotective Effects of PARP Inhibitors in Drosophila Models of Alzheimer's Disease. *Cells* **11**, (2022).

42. Michelena, J. *et al.* Analysis of PARP inhibitor toxicity by multidimensional fluorescence microscopy reveals mechanisms of sensitivity and resistance. *Nat Commun* **9**, (2018).

43. Montemorano, L., Michelle, D. S. & Bixel, L. K. Role of olaparib as maintenance treatment for ovarian cancer: The evidence to date. *OncoTargets and Therapy* vol. 12 11497–11506 Preprint at https://doi.org/10.2147/OTT.S195552 (2019).

44. Song, J. & Kim, J. Degeneration of dopaminergic neurons due to metabolic alterations and Parkinson's disease. *Frontiers in Aging Neuroscience* vol. 8 Preprint at https://doi.org/10.3389/fnagi.2016.00065 (2016).

List of published research papers and conference presentations

Peer-Reviewed Research & Review articles:

1. **Sarkar, A.**, Dutta, S., Sur, M., Chakraborty, S., Dey, P., & Mukherjee, P. (2023). **Early loss of endogenous NAD$^+$ following rotenone treatment leads to mitochondrial dysfunction and Sarm1 induction that is ameliorated by PARP inhibition**.*The FEBS journal*, *290*(6), 1596–1624. https://doi.org/10.1111/febs.16652
2. **Sarkar, A.**, Kumari, N., & Mukherjee, P. (2023). **The curious case of SARM1: Dr. Jekyll and Mr. Hyde in cell death and immunity?**. *The FEBS journal*, *290*(2), 340–358. https://doi.org/10.1111/febs.16256 **(featured in The FEBS journal cover issue)**
3. Das, S., Majumder, T., **Sarkar, A.**, Mukherjee, P., & Basu, S. (2020). **Flavonoids as BACE1 inhibitors: QSAR modelling, screening and in vitro evaluation**. *International journal of biological macromolecules*, *165*(Pt A), 1323–1330. https://doi.org/10.1016/j.ijbiomac.2020.09.232
4. Sur, M., Dey, P., **Sarkar, A.**, Bar, S., Banerjee, D., Bhat, S., & Mukherjee, P. (2018). **Sarm1 induction and accompanying inflammatory response mediates age-dependent susceptibility to rotenone-induced neurotoxicity**. *Cell death discovery*, *4*, 114. https://doi.org/10.1038/s41420-018-0119-5

Presentations and academic conferences/workshops:

- **Sarkar A,** Sur M, Dey P, Mukherjee P. **"**Early loss of NAD$^+$ following rotenone treatment is a key determinant of Sarm1 induction that is ameliorated by PARP1 inhibition". **Oral presentation** in National Conference organized by Society of Biological Chemists (I) & CSIR-Indian institute of Chemic Biology, Kolkata Chapter, 9th & 10th April, 2022.
- **Sarkar A,** Sur M, Dey P, Mukherjee P. **"**Parp1 inhibition ameliorates rotenone induced cell death by preventing NAD$^+$ dependent Sarm1 activation". **Presented poster** in 4th National Post doc Symposium, Scholars to pathfinders organized by IISER-Kolkata & India Bioscience (3-4 | 10-11 April, 2021).
- Participated in crafting your Career (CYC) workshop organised by India Bioscience conducted on September 20th, 2019 at Presidency University, Kolkata.
- **Sarkar A,** Dey P, Mukherjee P. "Inhibition of PARP1 rescue cells from death by inducing pro-survival mechanism under severe energy depletion." **Presented poster** in international Symposium on Frontiers in development & molecular medicine: models to insight organised by CSIR- Indian institute of Chemic Biology on 1st-3rd Merch, 2019, Biswa Bangla Convention Centre, Kolkata.